Variability and Dynamics of the Kuroshio and Mindanao Current during the 2010/11 La Niña and in Late 2012

BO LI,[a] DONGLIANG YUAN,[b,c] XIAOYUE HU,[d,e] YA YANG,[b,c] YAO LI,[c] AND SHIJIAN HU[c]

[a] *State Key Laboratory of Tropical Oceanography, Guangdong Key Laboratory of Ocean Remote Sensing, and Key Laboratory of Science and Technology on Operational Oceanography, South China Sea Institute of Oceanology, Chinese Academy of Sciences, Guangzhou, China*
[b] *Key Laboratory of Marine Science and Numerical Modeling, First Institute of Oceanography, Ministry of Natural Resources, and Shandong Key Laboratory of Marine Science and Numerical Modeling, Qingdao, China*
[c] *Key Laboratory of Ocean Circulation and Waves, Institute of Oceanology, Chinese Academy of Sciences, Qingdao, China*
[d] *Cooperative Institute for Marine and Atmospheric Studies, University of Miami, Miami, Florida*
[e] *NOAA/Atlantic Oceanographic and Meteorological Laboratory, Miami, Florida*

(Manuscript received 7 July 2023, in final form 29 March 2024, accepted 13 April 2024)

ABSTRACT: Variability of two Pacific western boundary currents (WBCs)—the Kuroshio and the Mindanao Current—during the strong 2010/11 La Niña event is investigated using ship-based hydrographic observations and moored current-meter data collected off the east coasts of the Philippines. The geostrophic currents calculated using the hydrographic data show that, during the 2010/11 La Niña winter, the Kuroshio decreased by ~10 Sv (1 Sv $\equiv 10^6$ m^3 s^{-1}), whereas the Mindanao Current increased by ~5–10 Sv, relative to the normal winter in late 2012. The interannual variability based on the hydrographic data is confirmed by moored current-meter measurements and satellite altimeter geostrophic currents. A coastally trapped Kelvin wave model is used to explain the interannual variability of the two WBCs during the different ENSO phases. The good comparison of the simulated sea level anomalies around the Philippines with the altimeter data suggests that the interannual variability of the WBCs is associated with Kelvin wave propagation from the Sulawesi–Sulu Seas clockwise around the Philippine Archipelago. We identified that the Kelvin waves are excited by downwelling equatorial Rossby waves propagating into the Indonesian Seas during the La Niña. The transport anomalies of the WBCs are comparable to the total meridional transport anomalies integrated across the interior North Pacific Ocean, suggesting the importance of the WBCs in the heat charge–discharge processes of the western Pacific warm pool during ENSO events.

SIGNIFICANCE STATEMENT: The two western boundary currents (WBCs)—the Kuroshio and the Mindanao Current—play the role of closing the subtropical and tropical gyre circulation of the Pacific Ocean. Their variability during ENSO is unknown. Existing studies based on numerical modeling suggest that their variability is highly correlated with ENSO, with the Kuroshio stronger and Mindanao Current weaker during La Niña and vice versa during El Niño. Here, we use in situ hydrographic observations combined with mooring and satellite altimeter data to show that the Kuroshio transport decreases and the Mindanao Current transport increases during the 2010/11 La Niña, the dynamics of which are controlled by the Kelvin wave propagation from the Sulawesi–Sulu Seas clockwise around the Philippine Archipelago. The result is important for the warm pool dynamics during ENSO.

KEYWORDS: Boundary currents; Kelvin waves; La Nina; Ocean dynamics; Transport

1. Introduction

The North Pacific Ocean circulation features western intensification, with the western boundary currents (WBCs) along the east Philippine coasts much stronger than the circulation in the interior basin. This phenomenon has been studied for over one-half of a century, leading to the births of the modern wind-driven ocean circulation theories (Sverdrup 1947; Stommel 1948; Munk 1950). An early description of the general ocean circulation in the Philippine Sea and in the southeast Asian marginal seas is given by Wyrtki (1961) based on historical data, showing that the North Equatorial Current (NEC) of the Pacific Ocean flows westward against the east Philippine coasts and splits into two WBCs, the Kuroshio and the Mindanao Current (MC). The detailed structure of the WBCs was not disclosed until the late 1960s during the cooperative study of the Kuroshio (CSK) (Nitani 1972). Later, the cooperative research program between the People's Republic of China and the United States during the Tropical Ocean and Global Atmosphere (TOGA) program made measurements of these WBCs along the periphery of a box east of the Philippines (Toole et al. 1990). The Western Equatorial Pacific Ocean Circulation Study (WEPOCS) project from 1985 to 1988 has conducted three surveys in the far western equatorial Pacific Ocean and uncovered an important structure of the MC and the New Guinea Coastal Current/Undercurrent (NGCC/UC) (Lindstrom et al. 1987; Lukas et al. 1991). Wijffels et al. (1995) summarized all of these cruises in the 1980s and early 1990s, based on which the mean circulation and transport of the MC were estimated. The low-latitude WBCs have been systemically observed during the past decade with the implementation of the Northwestern Pacific Ocean Circulation and Climate Experiment (NPOCE; Hu et al. 2011; Ma et al. 2022).

Earlier measurements of the WBC transports off the east Philippine coasts have mostly been made in boreal summer–fall

Corresponding author: Dongliang Yuan, dyuan@fio.org.cn

DOI: 10.1175/JPO-D-23-0124.1

(Toole et al. 1990; Hu et al. 1991; Lukas et al. 1991; Wijffels et al. 1995). The interannual anomalies of the Kuroshio and the MC at the mature phase of El Niño–Southern Oscillation (ENSO) events have rarely been obtained. Kashino et al. (2009) showed stronger MC and weaker Kuroshio in the late 2006 El Niño than in the early 2008 La Niña using shipboard acoustic Doppler current profiler (SADCP), but the dynamic height difference along the WBC sections in their hydrographic observations seems to suggest an opposite variation pattern. In addition, some other studies showed contrasting results. For example, Qu et al. (1998) reported a minimum transport of the NEC–Kuroshio–MC system during the mature phase of the 1986/87 El Niño and maximum transports in the years before and after the event. Hu and Hu (2014) suggested that the interannual variability of the NEC, observed by 16 years of repeated SADCP sections, is tied to the Niño-3.4 index but lags the latter by 6 months. In contrast, several other studies illustrated that the oceanic Niño index (ONI) has no significant simultaneous correlation with the upstream Kuroshio transport (Zhai and Hu 2013; Z. Chen et al. 2015). Using sea level records from tidal gauges, Lukas (1988) provided another example, finding that the fluctuations of the MC have no apparent relationship with the strength of ENSO.

Indeed, variations of the North Pacific WBCs during the mature phase of major ENSO events are not very well understood partly due to the scarcity of direct observations. Although limited, several mooring-based studies reported a strengthened MC after the onset of the 2002/03 El Niño (Kashino et al. 2005) and during the development of the 2015/16 El Niño from July to December 2015 (Liu et al. 2023). Using long mooring measurements, Hu et al. (2016) reported the weakest MC in June 2012, in contrast to maximum peaks in December 2010 and June 2014, with no significant relation found between the MC velocity and the Niño-3.4 index. Z. Chen et al. (2015) also reported a low correlation of 0.05 between the interannual surface velocity off the East Luzon coast and ONI, indicating that the interannual variations of the WBC do not always follow the ENSO cycle (Zhang et al. 2014).

The westward mass transport of the NEC splits into the northward and southward flows along the Philippine coasts. The NEC split latitude is estimated to be between 11° and 14.5°N at the sea surface and increases northward with depth (Nitani 1972; Toole et al. 1990; Qu et al. 1998, 1999; Qu and Lukas 2003). Existing modeling studies have suggested that the interannual variations of the NEC split latitude should be highly correlated with ENSO, moving northward during El Niño and southward during La Niña (Qiu and Lukas 1996). Therefore, the Kuroshio transport is expected to decrease and the MC transport to increase during El Niño, and vice versa during La Niña (Kim et al. 2004). These modeling studies thus suggest that the WBCs in the North Pacific Ocean counter the recharge and discharge of equatorial Pacific warm water volume by the interior Sverdrup circulation during ENSO events.

With the advent of sea level measurements by satellite altimeters, variations of the NEC split latitude have been investigated using the altimetry-derived surface geostrophic currents (Wang and Hu 2006; Qiu and Chen 2010). The interannual NEC split variations derived from the altimeter data are similar to those derived from previous numerical simulations. However, the altimeter data, especially the early Topex/Poseidon data, do not resolve the WBCs well and they suffer from a lack of subsurface information. A comprehensive validation of the altimeter analysis and the numerical-model-based results with in situ hydrographic observations is required.

Existing studies have attributed the interannual NEC split variations to the propagation of the wind-driven Rossby waves from the interior North Pacific (Qiu and Lukas 1996; Kim et al. 2004; Qiu and Chen 2010; Zhai and Hu 2013). However, the interactions of the NEC–Kuroshio–MC system with the circulation in the South China Sea (SCS) and the Indonesian Seas have not been taken into consideration. An earlier modeling study by Metzger and Hurlburt (1996) has suggested a coupled western Pacific–SCS circulation, which was later shown to be associated with the Kelvin wave propagation into the SCS along the west Philippine coasts based on the altimeter data (Liu et al. 2011; Zhuang et al. 2013). A recent modeling study has suggested that the Mindoro–Sibutu pathway is the gateway for the Kelvin waves to propagate clockwise around the Philippines from the western Pacific Ocean into the SCS (M. Li et al. 2021). Nevertheless, it is still unclear if the Kelvin waves can reach the east coasts to impact the NEC splitting and the WBCs in the presence of the strong Kuroshio in the Luzon Strait in reality.

Earlier studies of ENSO dynamics have demonstrated that interannual variations of the tropical Pacific Ocean circulation play an important role in sea surface temperature variability and global atmospheric circulation (Clarke 2008; Sarachik and Cane 2010; Hu et al. 2015). The existing theory has hypothesized the anomalous Sverdrup interior circulation discharge or recharge of the equatorial warm water volume and heat content during El Niño or La Niña, respectively (Jin 1997a,b). However, the potential effects of the WBCs on the recharge/discharge of the warm pool and the tropical climate variations have been overlooked so far.

Since 2010, multiple research cruises on an annual basis have been conducted to survey the northwestern Pacific Ocean. Among them, two cruises were carried out during late 2010, the mature phase of a strong La Niña, and late 2012 under a neutral ENSO condition. The surveys made measurements along the 18° and 8°N sections off the east Philippine coasts, which represent the source region of the Kuroshio and the MC, respectively. The variability of the WBCs in a La Niña winter in comparison with a normal winter is evaluated in this study.

2. Data and methods

The data used in this study include ship-based hydrographic data during the research cruises, density profiles from the international Argo project, satellite altimeter data, and long time series of moored current-meter data. The analyses of these data have resulted in consistent WBC transport variations.

TABLE 1. Time windows of the sectional surveys.

	18°N	8°N	130°E	8°N (second visit, 128°E west)
2010	20–26 Nov	2–5 Dec	20–24 Dec	17–18 Dec
2012	25–27 Nov	8–10 Dec	5–12 Dec	—

a. Hydrography data

The periods of the two comparative cruises are late November through December of 2010 and 2012, corresponding to the 2010/11 La Niña winter and a normal late 2012 winter (Table 1). Based on the Niño-3.4 index calculated as the average sea surface temperature anomalies in the area of (170°–120°W, 5°S–5°N) of the NOAA OISST.v2 dataset, the 2010/11 La Niña is one of the strongest La Niña events in the recent few decades (Fig. 1a). The difference of the ocean circulation between the two winters may represent the interannual anomalies during the strong 2010/11 La Niña peak to a certain extent.

The research cruises were carried out on board research vessel (R/V) *Kexue-1* using a SeaBird 911/917 plus conductivity–temperature–depth (CTD) sensor manufactured by the SeaBird Electronics (SBE), Inc. to measure ocean temperature and salinity profiles. CTD sectional casts were made along 18°N, 8°N, and 130°E in the western Pacific Ocean, which represent the states of the Kuroshio origin, the MC, and the NEC in the western Pacific in the two winters (Figs. 1b,c).

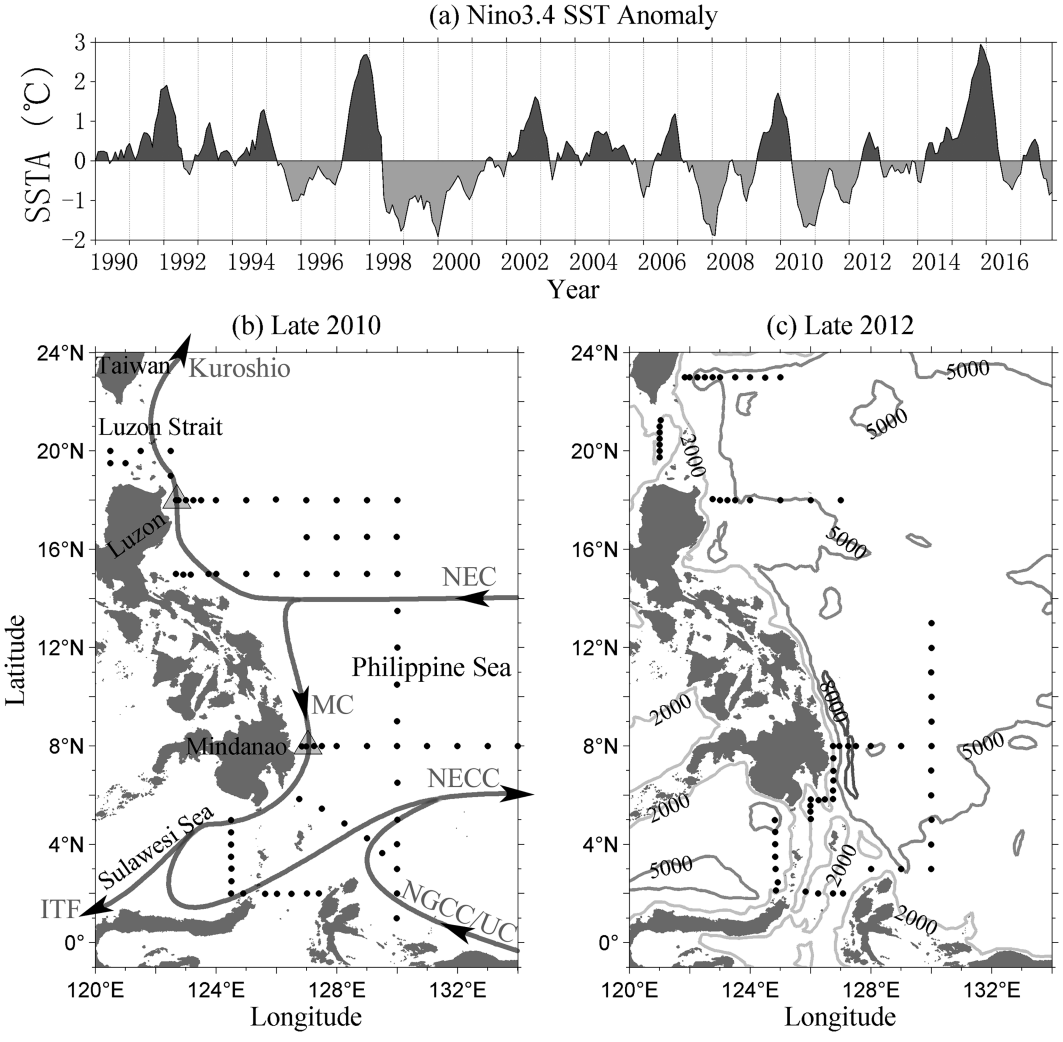

FIG. 1. (a) Niño-3.4 index based on the OISST.v2 dataset, showing a La Niña state in the winter of 2010 and a normal state in the winter of 2012. The unit is degrees Celsius. (b) CTD stations (black dots) during the winter cruises of 2010. Arrows and triangles indicate the general flow pattern and locations of subsurface moorings, respectively. (c) As in (b), but for the winter 2012 cruise. Contours in (c) are water depths in meters.

The raw CTD downcast data were processed using the manufacturer's software, averaged into 1-dbar pressure bins in the vertical, and interpolated onto a 0.25°-interval zonal grid in the 8° and 18°N sections and onto a 1°-interval meridional grid in the 130°E section using the Akima interpolation (Akima 1970).

b. Geostrophic currents

The geostrophic currents of the WBCs are calculated in reference to the 2000-dbar level of no motion. The currents in the upper layer above the pycnocline are not sensitive to the choice of the level of no motion deeper than 1500 m (Hu et al. 2021). The subsurface geostrophic currents are sensitive to the choice of the reference level, and their transports are, therefore, not estimated in this paper. The dynamic height near the sea bottom, where the water depth is less than 2000 dbar, was assumed to be the same as the nearby seaward station, which is equivalent to assuming a zero bottom geostrophic velocity.

The CTD sections along 18° and 8°N stop at about 0.25°–0.5° from the coast. The currents between the coast and the westernmost station of the section are interpolated using the Akima method assuming the nonslip condition at the coast. A comparison of the Akima interpolation within ~0.5° from the coast with the Munk WBC model, assuming a horizontal mixing coefficient of 800 $m^2\ s^{-1}$ (Lien et al. 2014), suggests an error of about 8.84% in the transport estimate, which is small.

c. Moored ADCP data

During the 2010 winter cruise, two moorings were deployed east of the Philippine coast and were later retrieved and redeployed in July 2011 (represented as triangles in Fig. 1b). Following the recovery of the second set of moorings during the 2012 winter cruise, the duration of direct measurements extended to nearly 2 years. With a 75-kHz upward-looking ADCP at a 700-m nominal depth, the north mooring was deployed in the Kuroshio at 18°N, 122.7°E on 20 November 2010. The instruments were redeployed on 11 July 2011 and recovered on 30 October 2012, with both upward- and downward-looking ADCPs at about 500-m depth during the second deployment. The south mooring at 8°N, 127.05°E was equipped with upward- and downward-looking 75 kHz ADCPs at 500-m depth for MC observation from 1 December 2010 to 7 December 2012, with one retrieval and redeployment on 15–16 July 2011. ADCPs measured velocity in 60 8-m bins every 1 h or 30 min. For more details, please see Hu et al. (2013), Zhang et al. (2014), and Z. Chen et al. (2015).

Daily averages were calculated from the original velocity measurements of these moorings for further analysis. The data shallower than 50 m were discarded due to contamination from reflection at the surface. This double-mooring dataset provides an unprecedented opportunity to investigate the synchronous variations of the two WBCs.

d. Argo profiles and absolute geostrophic currents

The Argo profile data of the upper 2000 dbar were downloaded from the China Argo Real-time Data Center. We use those profiles concurrent to the cruise period from November through December of 2012 to supplement the missing CTD casts in the vicinity of 18°N, 130°E (Fig. 1b). The Argo profiles are densely distributed in the northeastern corner of the box in November–December of 2012. The Argo profiles within 45 km of the CTD stations (128°–130°E along 18°N and 14°–18°N along 130°E with a 1° interval) were used to fill the missing data. Weighted averages of the spatially uneven distributed Argo profiles according to their inverse distance within 45 km from each CTD station are used to calculate the geostrophic currents. Since both kinds of the instruments are equipped with the sensors of the same SBE Company, e.g., SBE 911 or 917, the system errors between Argo and CTD profiles can be negligible. The error induced by the combination of the CTD and Argo data in the corner is not important because 1) the currents offshore is much weaker than in the WBCs, as evidenced by the CTD and altimeter data and 2) the pressure is continuous so that the error does not contribute to the residuals of the mass budget of the box.

A set of monthly gridded Argo data by Roemmich and Gilson (2009), which includes salinity and temperature profiles of the upper 2000 dbar at a 1° spatial resolution, were used to estimate the geostrophic meridional transport of the interior Pacific Ocean gyre. Absolute geostrophic currents (AGCs) were calculated from the gridded data using the P-vector method (Chu 1995), showing good agreement with the altimeter geostrophic currents at the sea surface and with moored current-meter measurements at a few locations in the tropical North Pacific Ocean (Yuan et al. 2014).

e. Satellite altimeter data

The satellite altimeter sea level L4 product was distributed by the Copernicus Marine Environment Monitoring Service (CMEMS) in November 2022. The product is processed with the CNES/CLS Data Unification and Altimeter Combination System (DUACS). The delayed-time, merged, global ocean gridded absolute dynamic topography (ADT, sea surface height above geoid) and the absolute surface geostrophic velocity of the dataset are adopted in this study. The data have a 1/4° × 1/4° Mercator spatial resolution and a 1-day temporal resolution. The daily data were monthly averaged for further analyses. The sea level anomalies (SLAs) were then calculated by referencing the ADT to the monthly climatology data spanning the period of 1993–2021.

f. Transport of the WBCs derived from ADT

In the tropical Pacific, the ocean circulation can be approximated by a 1.5-layer reduced gravity model, given the existence of a strong pycnocline that separates the upper layer from the abyssal ocean. Near the western boundary, the velocity of the WBC, including all of the locally and remotely forced currents, is governed by the geostrophic balance:

$$fv = g'\frac{\partial h}{\partial x} \tag{1}$$

where v is the meridional velocity, f is the Coriolis parameter, h is the upper-layer thickness, $g' = g(\Delta\rho/\rho)$, g is the gravitational

acceleration, ρ is the seawater density, and $\Delta\rho$ is the density difference between the upper and abyssal layers. From Eq. (1), we can calculate the meridional transport of the WBC as

$$Q = \int_{x_w}^{x_w+L} vhdx = \int_{x_w}^{x_w+L} \frac{g'}{2f}\frac{\partial h^2}{\partial x}dx$$
$$= \frac{g'}{2f}[h^2(x_w + L) - h^2(x_w)],$$

where x_w is the coordinate of the western boundary and L is the width of the WBC. Considering $\eta = (g'/g)h$ in the reduced gravity model, Q is calculated as

$$Q = \frac{g\rho}{2f\Delta\rho}[\eta^2(x_w + L) - \eta^2(x_w)], \quad (2)$$

where η is the vertical displacement (positive upward) of the sea surface, which can be represented by the ADT anomalies. The squared difference of the sea level ($\Delta\eta^2$) across the WBC is thus used to represent the WBC transport, the interannual anomalies of which are analyzed in our paper. With $f = 10^{-4}$ s^{-1}, $\rho = 1000$ kg m^{-3}, $\Delta\rho = 1$ kg m^{-3}, and $g = 10$ m s^{-2}, a 0.2-m^2 $\Delta\eta^2$ difference across the WBC corresponds to a transport anomaly of about 10 Sv (1 Sv $\equiv 10^6$ m^3 s^{-1}).

g. *The linear coastally trapped Kelvin wave model*

The Kelvin wave model is based on the analytical linear wave model described by Gill (1982) and forced by wind stress along the Kelvin wave pathway. Sprintall et al. (2000) and Hu et al. (2019) used the model to predict the sea level variations in the Indonesian Seas associated with the propagation of Kelvin waves. In this study, we employ the same model to investigate the sea level propagation around the Philippine coasts forced by the Kelvin waves and the local winds. The model integrates the momentum equation in the alongshore direction x as follows:

$$\frac{dA_k}{dt} + c\frac{dA_k}{dx} = \frac{cX}{g}. \quad (3)$$

Here, A_k represents the SLA along the Kelvin wave characteristic line, X denotes the alongshore wind stress projected onto each baroclinic mode, and g is the acceleration due to gravity. The first 10 baroclinic modes decomposed from the ERA5 ocean dataset are used in this study. The wave speed of the first baroclinic mode c is 3.0 m s^{-1} near the Philippines (Chelton et al. 1998). We replace x with $t = x/c$, allowing the integration of Eq. (3) along the Kelvin wave characteristics to yield the solution of A_k at any location along a Kelvin wave pathway at any given time.

3. Results

In this section, the NEC–Kuroshio–MC system and its variations are analyzed based on the geostrophic currents and the moored current-meter data, combining with satellite data.

a. *The NEC–Kuroshio–MC system in the in situ observation*

The two surveys were conducted in nearly the same calendar days of the two winters of 2010 and 2012, between which the subsurface moorings equipped with ADCPs measured the WBC velocity at designated places. These data provide an unprecedented opportunity to examine the interannual variations of the NEC–Kuroshio–MC system.

1) GEOSTROPHIC CURRENTS IN THE 18°N SECTION

The distributions of temperature, salinity, and geostrophic currents in reference to the 2000-m level of no motion in the 18°N section in these two winters are shown in Fig. 2. Two density levels of 24.7σ_θ (i.e., potential density minus 1000 kg m^{-3}) and 25.8σ_θ, roughly overlapping with the 20° and 14°C isotherms, respectively, represent the upper and lower limits of the pycnocline (Meyers 1979; Kessler and Taft 1987). The density of 26.7σ_θ, which is traditionally used as the bottom of the WBCs, is also used to estimate the WBC transports (Qu et al. 1998).

The width and magnitude of the Kuroshio origin during the 2010/11 La Niña winter in the 18°N section are noticeably smaller than those in the winter of late 2012, suggesting that the strength of the Kuroshio in the origin decreases during the La Niña event (Figs. 2a,b). The differences of the meridional geostrophic currents in the 18°N section between the two winters (Fig. 2c), representing the WBC anomalies during the La Niña winter, are predominantly negative, suggesting that the Kuroshio origin is weakened significantly during the 2010/11 La Niña mature phase.

The geostrophic transports are integrated from the Philippine coast offshore, which bring the transports back to its mainstream value after crossing eddies. The integrated meridional transports above the 25.8σ_θ density surface from the western boundary clearly show that the transport of the WBC west of 124°E is about 6 Sv in the winter of late 2010, 11 Sv smaller than in the winter of late 2012. The 25.8σ_θ density surface is chosen because of its proximity to the ocean thermocline, above which is the wind-driven circulation important for ENSO dynamics. The weakening of the Kuroshio origin transport in 2010 is also confirmed by the transport calculation above the 24.7σ_θ and 26.7σ_θ surfaces.

2) GEOSTROPHIC CURRENTS IN THE 8°N SECTION

In comparison, the speed and width of the southward MC are larger in the winter of late 2010 than in the winter of late 2012 in the 8°N section (Fig. 3). The difference of the meridional geostrophic currents in the 8°N section shows predominantly southward anomalies in the upper layer, suggesting a strengthened MC in the 2010/11 La Niña winter. The integrated meridional transport above the 25.8σ_θ density surface from the western boundary shows that the transport of the MC west of 129.25°E is about 10 Sv larger in the winter of late 2010 than in the winter of late 2012.

In the subsurface, the geostrophic currents show a northward current offshore in the late 2010 winter, which could be

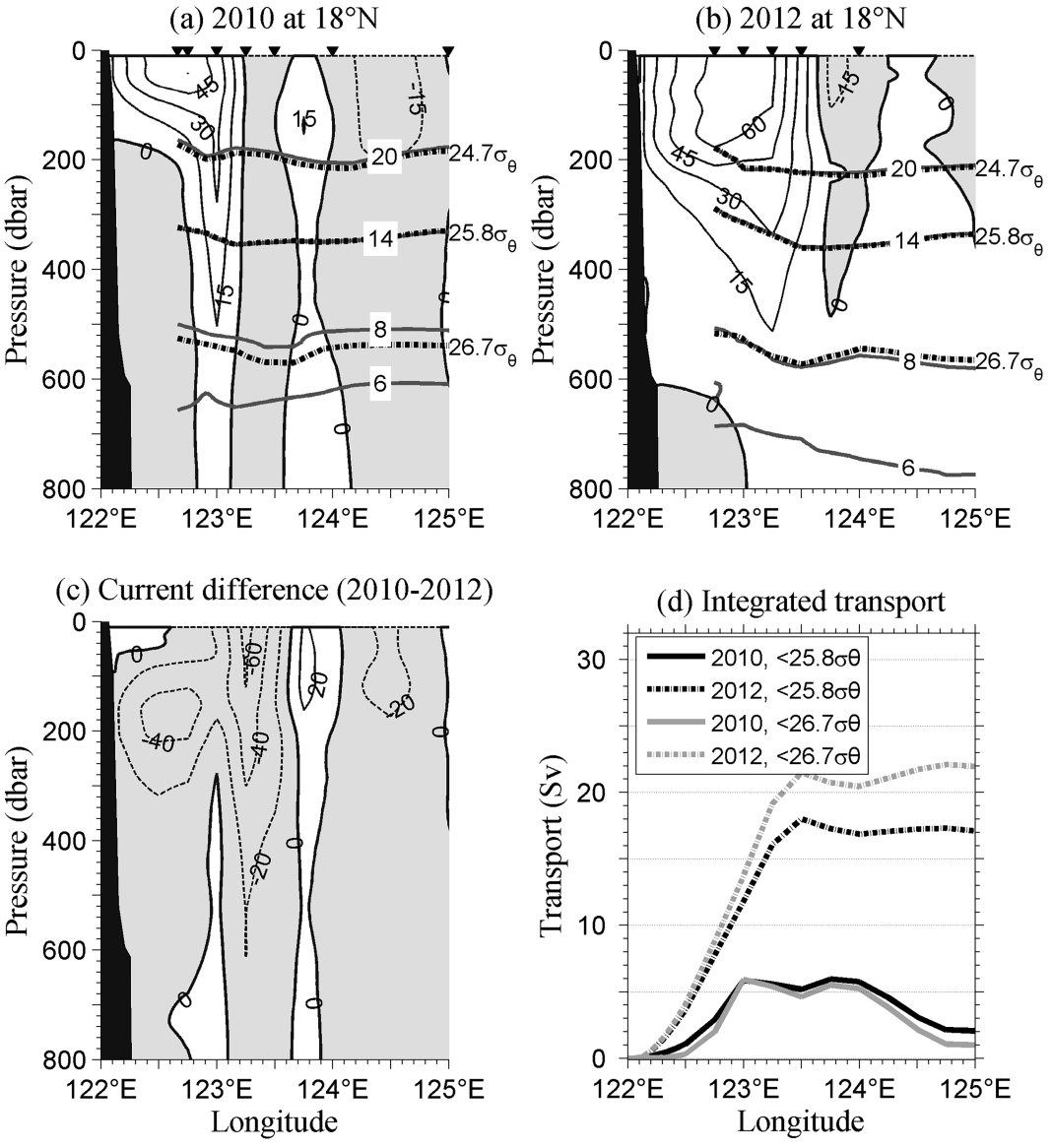

FIG. 2. Distribution of potential temperature (°C; thick contour) and meridional geostrophic currents (cm s^{-1}; thin contour) in the 18°N section in the winters of (a) 2010 and (b) 2012. The geostrophic currents are in reference to the 2000-m level of no motion. (c) The difference of the meridional geostrophic currents of the two winters. Solid (dash) contours indicate the northward (southward) currents. Solid-gray curves mark the potential temperature. The 24.7$\sigma\theta$, 25.8$\sigma\theta$, and 26.7$\sigma\theta$ density surfaces are plotted in the dot–dash curves in (a) and (b). (d) The integrated transports (Sv) above the 25.8$\sigma\theta$ and 26.7$\sigma\theta$ density surfaces from the western boundary. The gray shading in (a)–(c) indicates the southward flow. The black shading on the left in (a)–(c) indicates the continental slope.

the Mindanao Undercurrent (Hu et al. 1991) or a part of an anticyclonic eddy (Kashino et al. 2015). The core of this current shifted eastward in the winter of late 2012, suggesting significant variability of this subsurface flow.

During the late 2010 winter survey, the westernmost four stations of the 8°N section were visited for the second time about 2 weeks after the first visit. The geostrophic currents of the second visit also show a stronger MC southward in the upper layer and anomalous northward currents in the subsurface than in the winter of late 2012 (Fig. 4). The southward transport of the MC west of 128°E and above the 25.8σ_θ density surface has exceeded 20 Sv, showing an increase of more than 10 Sv from the winter of 2012. The currents in this section were different during the two visits in December 2010 because an eddy was present during the first visit (Fig. 3a). The existence of the eddy, centered at 7.5°N, 128.1°E, was confirmed by satellite sea level data during 4–10 December, with its position nearly fixed during the 1.5 days of the first visit (figure omitted). The integrated transport, with a hiccup at 127.25°–127.5°E due to the presence of the eddy, approaches

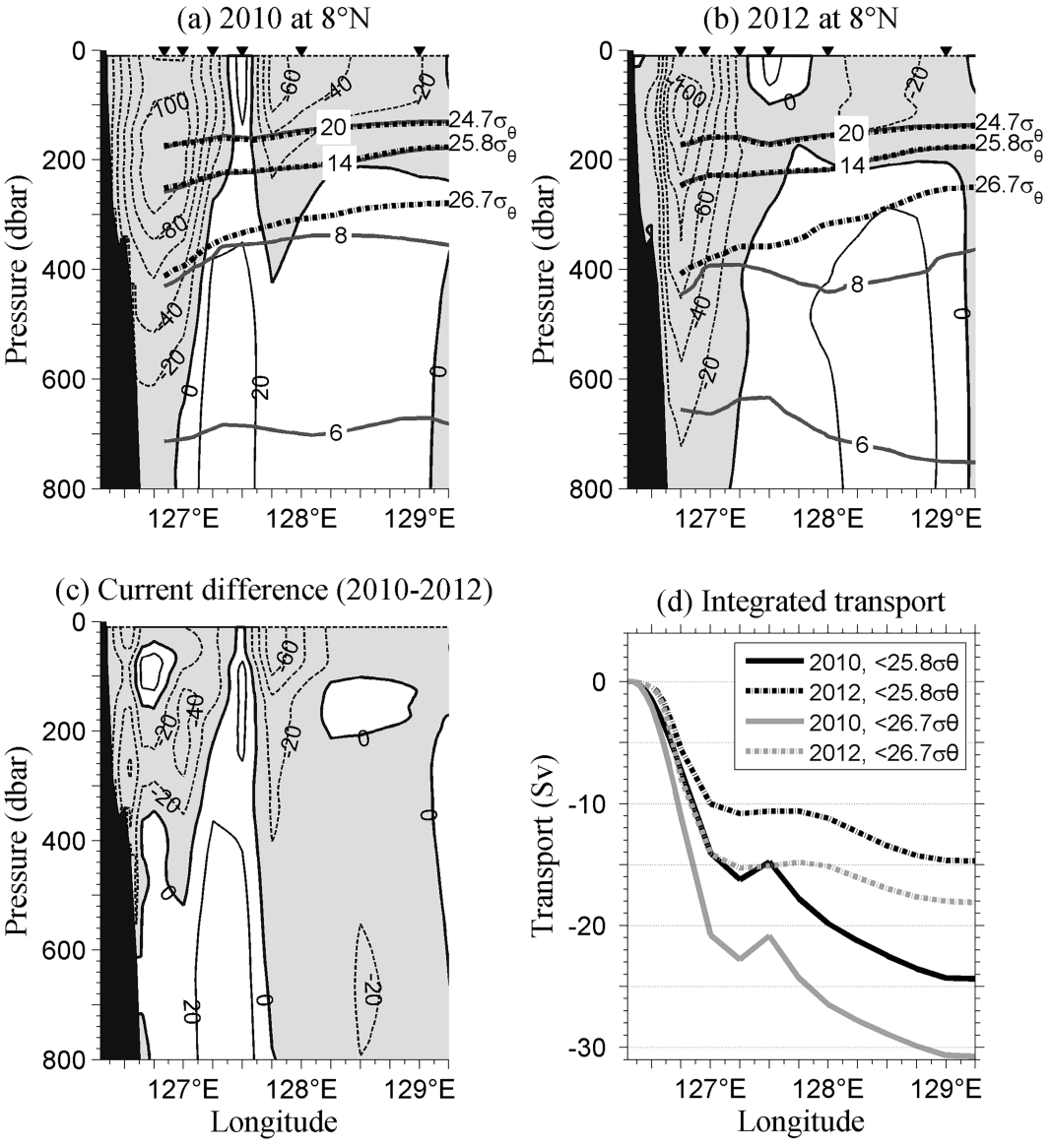

FIG. 3. As in Fig. 2, but for the 8°N section.

the maximum at 129.25°E asymptotically, suggesting the total WBC transport. No eddy was present in this section in the second visit. The integrated transport increases monotonically offshore from the boundary, reaching a maximum at 128.0°E, nearly equal to the transport of 30 Sv above 26.7σ_θ in the first visit. The comparison suggests that the offshore integration of the geostrophic currents is able to eliminate the eddy effects on WBC transports. The transport estimates in the two visits suggest consistently that the MC in 2010 is stronger than that in 2012.

3) DYNAMIC HEIGHTS OF THE NEC–KUROSHIO–MC SYSTEM

The dynamic heights relative to 1000 dbar along the 18°N, 8°N, and 130°E sections are shown in Fig. 5. This figure can be compared with Fig. 3 in Toole et al. (1990) and with Fig. 4 in Kashino et al. (2009). The gradients of the dynamic heights indicate the magnitude of shallow geostrophic currents across each section. The dynamic height variations along 18° and 8°N sections over the two cruises are quite pronounced, especially near the boundary. The net height changes during the late 2010 winter are smaller in the 18°N section and larger in the 8°N section than in the late 2012 winter, suggesting a weaker Kuroshio and a stronger MC in the late 2010 La Niña winter than in the late 2012 normal winter. A stronger MC and a weaker Kuroshio off the east Philippine coasts during late 2010 than those during late 2012 can also be inferred from the zonal ADT gradient along 8° and 18°N, respectively, averaged from November to January (Li et al. 2018). The results show that a robust interannual variation of the WBCs is

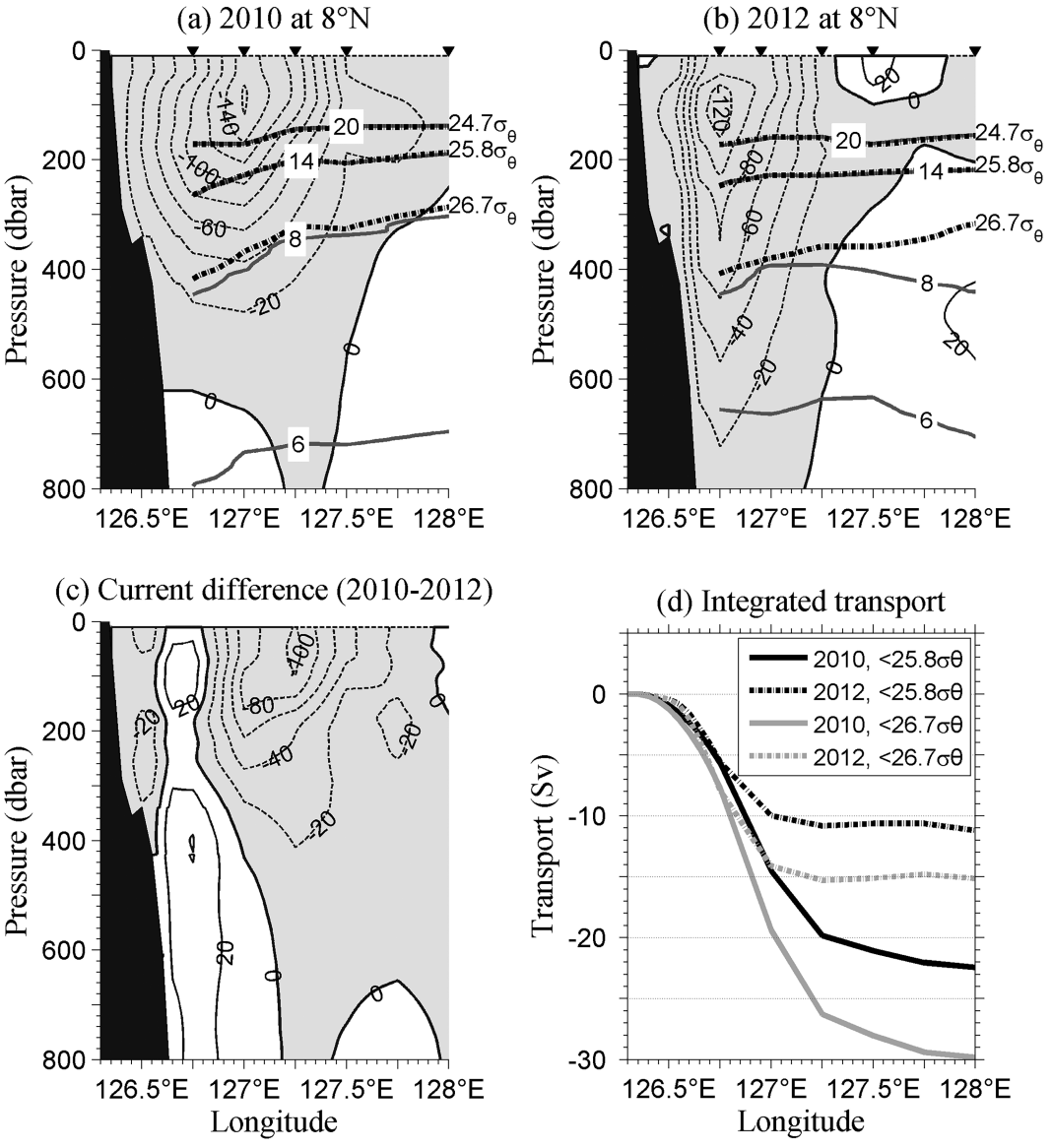

FIG. 4. As in Fig. 3, but for the second visit of the 8°N section of the late 2010 winter.

present, consistent with the diagnosed results based on the geostrophic currents of the in situ CTD data.

The interannual variability of the sectional WBC transports in this study is different from that of Toole et al. (1990), showing stronger transports of the NEC, the Kuroshio, and the MC in the spring of 1988 during a cold phase of ENSO than in the fall of 1987 after the 1986/87 El Niño. Kashino et al. (2009) suggested that the differences of the three currents shown by Toole et al. (1990) were mostly associated with the seasonal variability in this region and due to a cyclonic eddy located at the northernmost part of the 130°E section. Our analysis is consistent with the dynamic height calculation by Kashino et al. (2009), implying a stronger Kuroshio and a weaker MC during El Niño events than during La Niña events.

4) MOORING MEASUREMENTS OF THE WBCS

In the northern mooring's first deployment at 18°N, 122.7°E east of Luzon, the upward-looking ADCP cover the depth below about 200 m. Thus, this study analyzes the Kuroshio transport below this depth. The vertically averaged velocity between 200 and 350 m exhibits a continuous strengthening trend of the Kuroshio origin from November 2010 to October 2012 (Fig. 6a), which is in agreement with the analysis by Z. Chen et al. (2015). The current-meter observation is consistent with the 18°N geostrophic flow showing that the Kuroshio was weakened during the La Niña winter of 2010/11 compared to the normal winter of late 2012 (Fig. 2).

The mooring in the MC was deployed east of the Mindanao Island at 8°N, 127°E. As seen in Fig. 6b, the vertically averaged

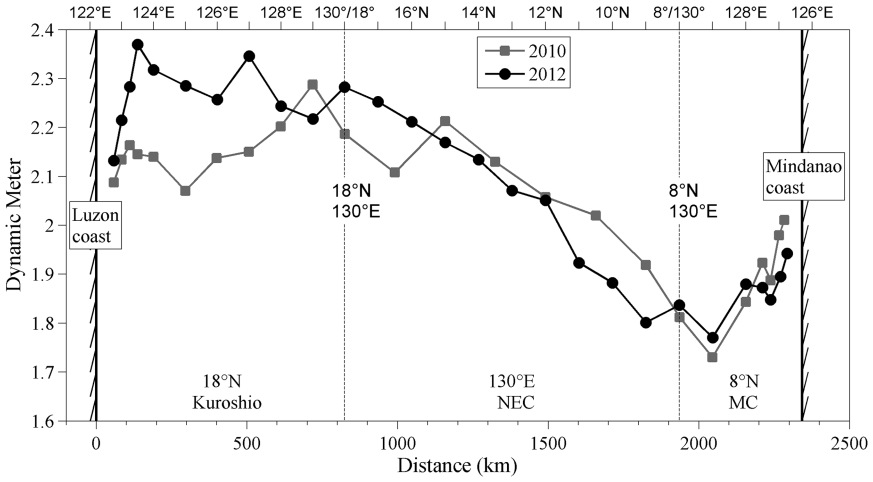

FIG. 5. Dynamic height along the 18°N, 8°N, and 130°E sections relative to 1000 dbar in the winter of 2010 (square) and 2012 (dot). The bottom x axis indicates the distance from the East Luzon coast at 18°N along the boundary of the box surrounded by 18°N, 8°N, and 130°E sections, with the longitudes/latitudes marked in the top x axis. The two feathered vertical lines at the ends mark the east coasts of the Philippines at 18° and 8°N, respectively. The two dotted vertical lines in the middle indicate the corners of the box.

velocity series above 200 m and its linear trend indicate clearly that the MC is stronger in the winter of 2010/11 La Niña than in the winter of late 2012, which is consistent with the geostrophic calculations in the 8°N section (Figs. 3 and 4). This mooring was maintained to cover the period until August 2014, with which Hu et al. (2016) reported the weakest MC observed in June 2012, in contrast to maximum peaks in December 2010 and June 2014.

5) VARIATION OF THE NEC SPLIT LATITUDE

The movement of the NEC split latitude is estimated based on a volume budget of a box surrounded by the Philippine coast and the 8°N, 18°N, and 130°E sections (Fig. 7). The CTD profiles north of 13°N in the 130°E section and east of 127°E in the 18°N section in 2012 are complemented with nearby Argo profiles in November and December 2012. The top-up and top-down triangles in the 130°E longitude mark

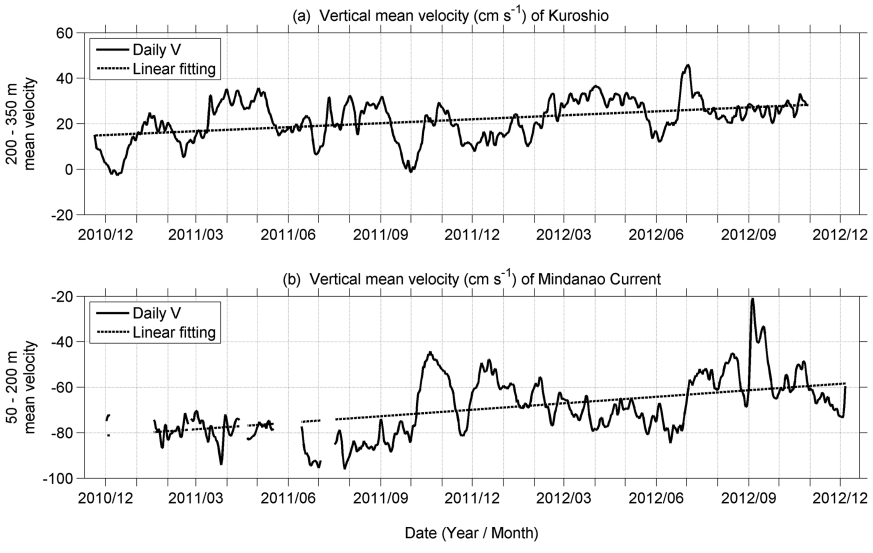

FIG. 6. Vertically averaged daily meridional velocity (cm s^{-1}) (a) between 200 and 350 m from the 18°N, 122.7°E mooring and (b) between 50 and 200 m from the 8°N, 127.05°E mooring. The time series has been smoothed by a 3-day running mean filter, with the linear trend plotted in the dashed line. The trends both exceed 95% significance level according to the Mann–Kendall test (Hamed and Ramachandra Rao 1998). The abscissa is the time in year/month.

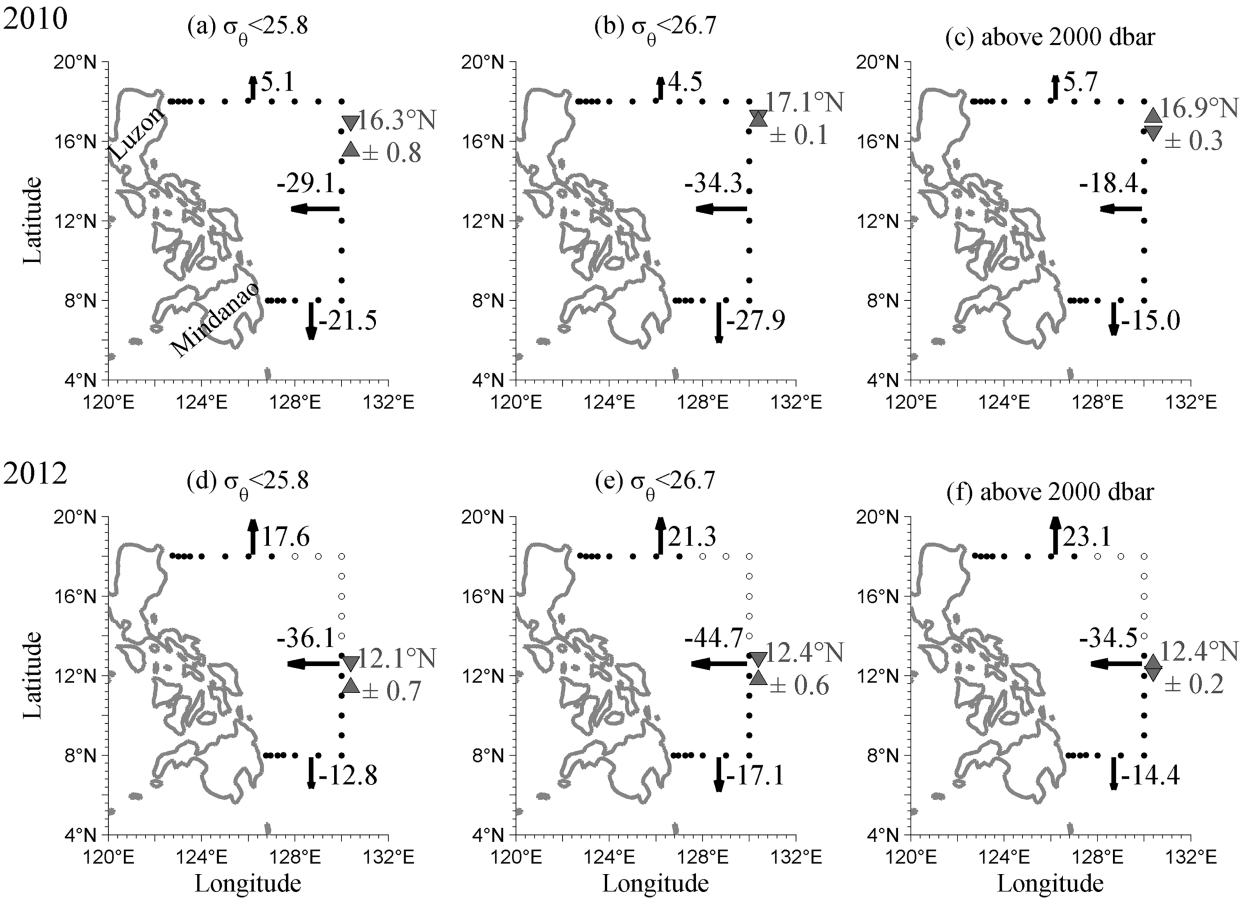

FIG. 7. Comparison of the geostrophic transport budgets above different isopycnic surfaces within a box east of the Philippines in the winters of (a)–(c) 2010 and (d)–(f) 2012. Dots mark the hydrographic stations of the survey. Data at the circles in the northeastern corner of the box are averaged from the nearby Argo profiles within 45 km during November through December of 2012. The numbers and arrows at the boundaries indicate the magnitudes and directions of the volume transports across the sections. Unit of transports is 10^6 m^3 s^{-1}. The top-up and top-down triangles in 130°E mark the positions of zero value transports integrated from the Philippine coast along the southern (8°N and 130°E) and northern (18°N and 130°E) peripheries of the box, respectively. The middle of the triangles in the 130°E section is taken as the mean NEC split latitude. The distance between them is the uncertainty of the NEC split latitude estimate, resulting from surplus of the volume transport of the upper ocean.

the points of zero transport integrated from the Philippine coast along the southern (8°N and 130°E) and northern (18°N and 130°E) peripheries of the box, respectively. The volume budget above the 2000-dbar reference level of no motion is essentially closed. The budget suggests that the split latitude of the NEC above the 25.8σ_θ isopycnic surface is in the range of 12.1°N ± 0.7° along the 130°E section in the winter of late 2012 and has moved northward to 16.3°N ± 0.8° during the La Niña winter of late 2010. This movement is larger than the uncertainty of the NEC split latitude estimates (0.7°–0.8°) based on the budget surplus of the box and is believed to be robust. A similar northward movement of the split latitude is also obtained based on the volume budget of the box above the 26.7σ_θ surface. This northward movement of the split latitude during a La Niña is contrary to the existing paradigm of the WBC interannual variability in the published literature (Kim et al. 2004; Qiu and Chen 2010; Zhai and Hu 2013).

The convergence and divergence of the volume transports above and below the 25.8σ_θ isopycnic surface in the box east of the Philippines in our study are 2.5 Sv in 2010 and 5.7 Sv in 2012, respectively. These are balanced by an average vertical velocity of 3.6–8.2 × 10^{-6} m s^{-1}, which is in the same order of magnitude as the 9.1 × 10^{-6} m s^{-1} vertical velocity estimate from the 1988 cruise reported by Toole et al. (1990). In 2012, the integrated transport across the 130°E section above 2000 dbar was nearly twice that of the late 2010 La Niña (Figs. 7c,f). In contrast, Toole et al. (1990) revealed the doubling of the NEC transport from September 1987 after a warm phase to April 1988 during a cold phase, which probably included significant seasonal variations (Kashino et al. 2009).

b. *Comparison with satellite altimeter data*

The surface geostrophic current and its estimated transport from satellite altimeter data (Fig. 8) show a weakened Kuroshio and an intensified MC during December 2010 compared

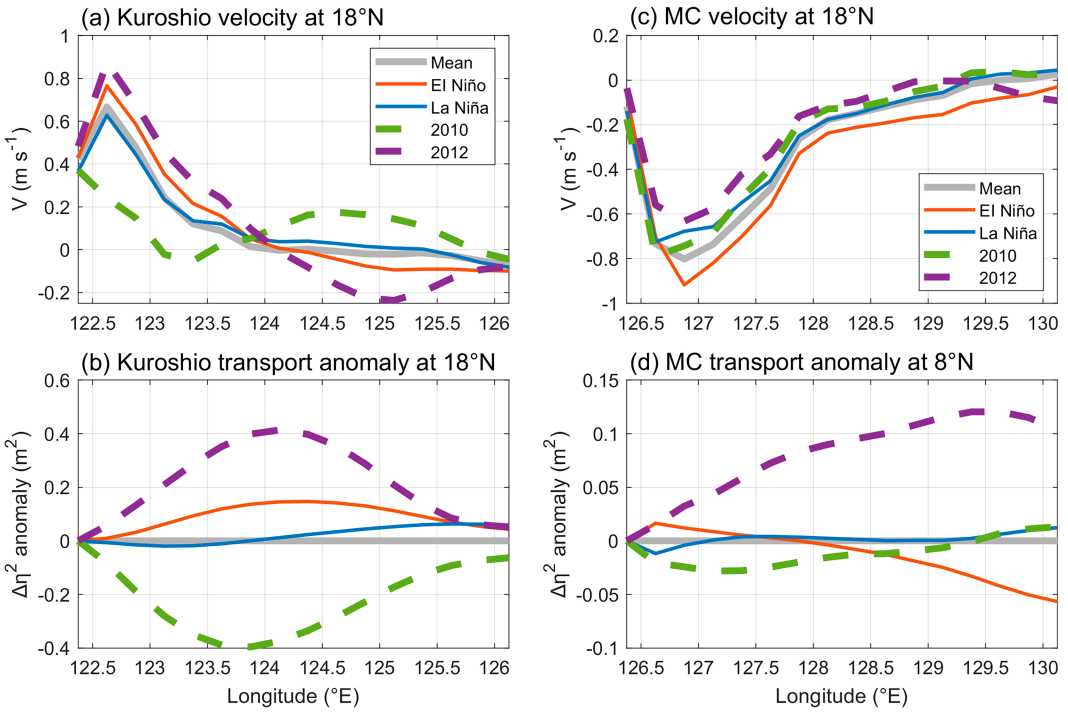

FIG. 8. Surface meridional geostrophic velocity in the (a) 18°N and (c) 8°N sections and cumulative sea level square differences ($\Delta\eta^2$) from the western boundary in the (b) 18°N and (d) 8°N sections. The $\Delta\eta^2$ anomalies in (b) and (d) are between adjacent grid points and are based on the climatology of 1993–2021. In each subplot, the thick gray is the December average from 1993 to 2021 and the dashed green and purple lines are Decembers of 2010 and 2012. Respectively, the orange and blue lines are the results of a composite analysis for the following ENSO periods: warm phase: December 1994, 1997, 2002, 2006, 2009, 2015, and 2018; cold phase: December 1995, 1998, 1999, 2007, 2010, 2011, and 2017.

to that of 2012, which are consistent with the geostrophic currents based on hydrographic data (Figs. 2–4) and direct measurements of the current meters (Fig. 6). Composite analysis indicates that, in December, the Kuroshio at 18°N and the MC at 8°N are strengthened during El Niño (orange lines in Fig. 8). The Kuroshio and the MC during the La Niña December (blue lines) are closer to the climatological average than during El Niño. Composite analysis based on five modeling datasets covering 10 warm events during 1980–2015 also suggested a strengthened MC in a developing El Niño (Ren et al. 2020).

Although composite analyses can reveal the WBCs' interannual anomalies related to ENSO, there is still significant uncertainty when it comes to an individual event. For instance, when compared to the multiyear average, December 2012 has shown considerably stronger Kuroshio and weaker MC (Fig. 8), suggesting that it is not a typical neutral WBC state (Li et al. 2018). Compared to the composite La Niña phase, the WBCs in December 2010 exhibit a significantly weaker Kuroshio and a relatively stronger MC, the dynamics of which need a separate study. It is worth mentioning that the along-track altimeter sea level can be used to calculate the geostrophic WBCs only if the satellite tracks are perpendicular to the western boundary. The various angles between the altimeter satellite tracks and the Philippine coasts suggest large uncertainties of the geostrophic WBCs derived from the altimeter data.

The time series of $\Delta\eta^2$ between adjacent grid points are calculated in the 18° and 8°N sections. The integrated anomalies of the $\Delta\eta^2$, representing the WBC transports in these sections, show a significant interannual variability not in close association with the ONI (Figs. 9a,b). The 13-month low-pass-filtered data indicate a strengthening Kuroshio and a weakening MC from late 2010 to late 2012, consistent with the mooring observations in Fig. 6. The correlation analysis between the WBC transport and ONI (including both Niño-3.4 and Niño-4 indices) reveals a weak correlation coefficient at the zero time lag and below the 95% significance level when the ONI leads the WBC anomalies (Figs. 9c–f). Similar results are presented by lead–lag correlation analyses between the integrated surface meridional velocity and the ONI (Figs. 9g–k). This implies that the WBCs east of the Philippine coasts do not vary with the ONI above the statistical significance.

4. Discussion

a. *Importance of the WBCs on ENSO*

The interannual WBC transports at 8°N have been compared with the meridional geostrophic transport anomalies integrated across the North Pacific Ocean based on Argo AGCs. In the

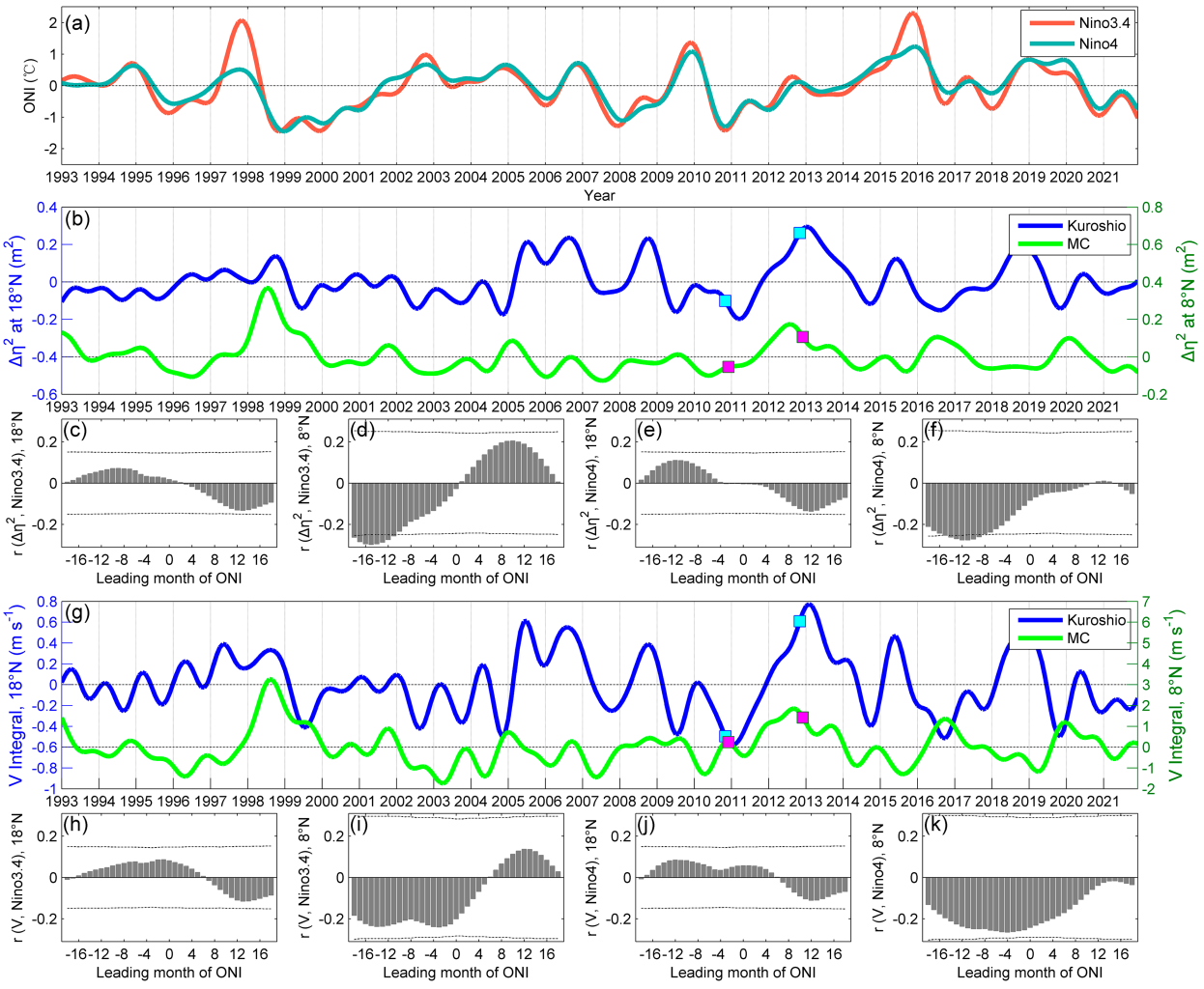

FIG. 9. Time series of (a) ONI, (b) $\Delta\eta^2$ anomalies across the WBCs, and (g) the integrated surface meridional velocity in the 18°N [blue line in (b) and (g)] and 8°N [green line in (b) and (g)] sections. The time series in (b) and (g) have been smoothed by a 13-month Butterworth low-pass filter from the monthly anomaly. Time nodes of the sectional observations during the two cruises are marked with squares. (c)–(f) Bar charts in represent the lead–lag correlation coefficient r between $\Delta\eta^2$ anomalies and ONI [Niño-3.4 in (c) and (d) and Niño-4 in (e) and (f)], and the 95% significance level in dash lines is based on the freedom degree of Bretherton et al. (1999). Positive lags here indicate the lead of ONI over the $\Delta\eta^2$ anomalies. (h)–(k) The same correlation analyses between the integrated surface meridional velocity and ONI are illustrated. The widths of the Kuroshio and the MC, L in Eq. (2), are selected as 2° and 3°, respectively, according to their V profiles in Figs. 8a and 8c.

layer above 400 m, the interior meridional geostrophic transports are found to recharge the equatorial Pacific heat content during the 2010/11 La Niña with negative transports (Fig. 10). The differences in the WBC transports of about 10 Sv southward anomalies between the two winters are evidently of the same magnitudes and have enhanced the interior recharging process during the 2010/11 La Niña. The comparison above the 20°C isotherm is essentially the same (figure omitted), suggesting that the WBC changes, which have been overlooked in the existing ENSO theories, are important for tropical–extratropical exchange of the Pacific Ocean at the interannual time scales.

b. Dynamics of the interannual WBC variations

The interannual anomalies of the WBCs are associated with SLA along the Philippine coasts during the La Niña, as evidenced by the satellite altimeter data in December 2010 (Fig. 11a). The SLAs around the Philippines are in positive correlations, above the 95% significance level, with those in the equatorial western Pacific (Fig. 11b). The strong correlations suggest that the sea level around the Philippine Archipelago should be affected by the signals from the tropical western Pacific Ocean. In comparison, the SLAs at the east Philippine coasts north of the bifurcation latitude are in poor correlation with the Rossby wave SLA coming from the east in the open ocean. Existing studies have suggested that oceanic signals from the Pacific Ocean can propagate into the eastern SCS through the Sibutu Passage and the Mindoro Strait as coastally trapped waves (Liu et al. 2011; Zhuang et al. 2013; X. Chen et al. 2015; M. Li et al. 2021).

Here, we extract the altimeter SLA data along the Rossby–Kelvin waveguide in the equatorial western Pacific around the

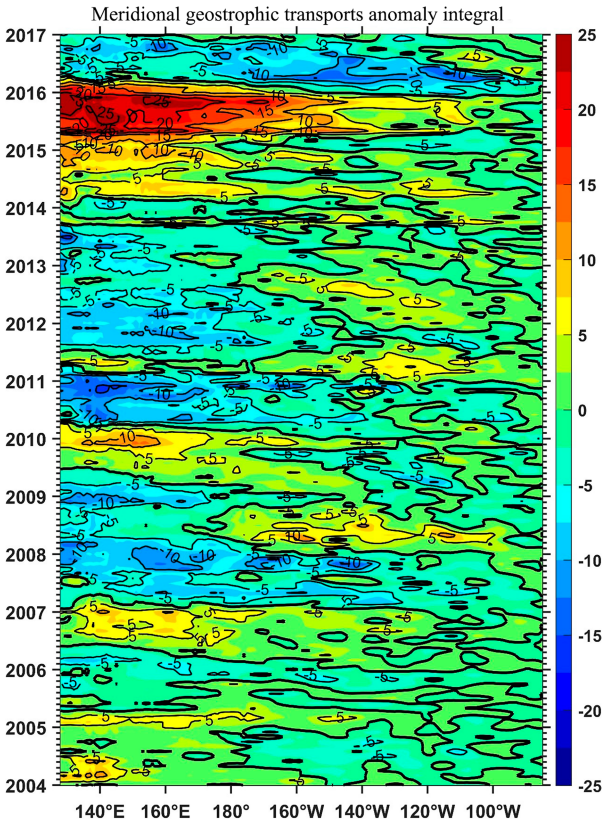

FIG. 10. Meridional geostrophic transport anomalies (Sv) integrated from the eastern boundary along 8°N. The transports are based on the Argo AGCs above the 400-m depth. The transport anomalies are based on the Argo climatology of 2004–16. The thick contour is the zero value.

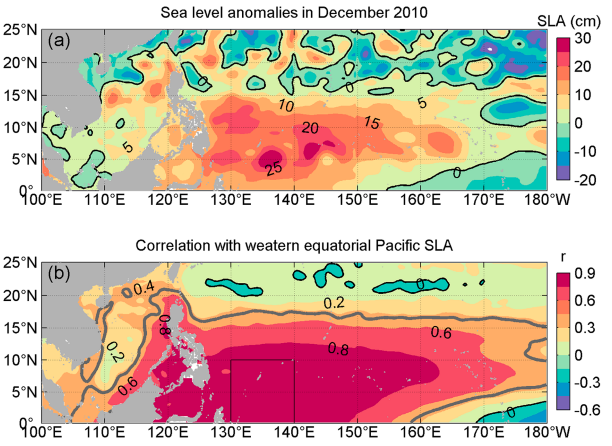

FIG. 11. (a) Interannual SLA (cm) of satellite altimeters in the northwestern Pacific Ocean in December 2010 based on the climatology of 1993–2021. (b) Correlation coefficients between the interannual SLA in the northwestern Pacific and those averaged in the western Pacific rectangle (0°–10°N, 130°–140°E). The gray contour in (b) marks the correlations at 95% significance level for 16 degrees of freedom, which correspond to the SLA freedom degree based on Bretherton et al. (1999) in the western Pacific rectangle.

Philippine Archipelago (Fig. 12). Before entering the Sulu Sea through the Sibutu and Balabac Passages, the SLAs propagate westward from the equatorial Pacific. The speed of the propagation (before station 22 in Figs. 12a,b) is about 1.21 m s^{-1}, consistent with the speed of the first baroclinic Rossby wave estimated as $c_r = \beta R^2$, with the deformation radius R of 230 km in the western tropical Pacific (Chelton et al. 1998). The Rossby wave propagation is blocked or interfered with by the WBCs, so their propagation near the boundary is meant to be different from the propagation in the open ocean. The SLAs enter the SCS via the Mindoro Strait and then return to the western Pacific via the Luzon Strait, completing the circum-island propagation around the Philippines (from station 22 to station 45 in Fig. 12c). A time lag of ~9 days is indeed indicated by the cross correlation between the SLA at stations 45–46, where the coastal SLAs are least aliased by mesoscale eddies coming from the east, and at stations 25–26. The propagation speed is in agreement with the phase speed of the Kelvin wave of ~3.0 m s^{-1} around 8°–18°N (Chelton et al. 1998). The Kelvin waves propagate very fast, and the monthly data and the coarse resolution of the satellite altimeter sampling in space and in time are prone to aliasing by mesoscale eddies. Fortunately, the eddy impingements are of intraseasonal durations and do not disrupt the synchronous interannual SLA around the Philippines fundamentally. The effects of all of the above make the SLA around the Philippines revealed as nearly synchronous positive or negative belts in the Hovmöller plot.

The altimeter data suggest that the dissipation of the Kelvin wave energy occurs mainly in the Sulawesi Sea and the Sulu Sea as passing through the Sibutu Passage (stations 18–25, Fig. 12b). After entering the SCS, the reduction of the Kelvin wave amplitudes is actually very small around the Philippines (stations 25–45). The Kelvin waves have evidently propagated across station 40 and arrived at the east Philippine coasts through the Luzon Strait to influence the WBC transports by inducing the interannual variability of $\Delta\eta^2$—the squared differences of the sea level across the WBCs. Traditional linear dynamics suggest that the Rossby waves arriving at the Philippine coast may excite the Kelvin waves to enter the Sulawesi Seas. Modern nonlinear interaction studies suggest that the Rossby waves are not able to penetrate through the strong potential vorticity barrier of the WBC in general. Instead, the Rossby waves are advected and distorted downstream by the WBC to dissipate into current anomalies, which determine the generation of the equatorial and coastal Kelvin waves in the Sulawesi Sea (Yuan and Wang 2011). Regime changes of the WBCs could be induced by such nonlinear interactions sometimes.

The altimeter data suggest that SLAs in the western Pacific have the highest variance at 5.375°N, which could enter the Sulawesi Sea directly. The first baroclinic equatorial Rossby waves have the largest sea level amplitudes at about 5°–7°N. These SLAs east of the Mindanao Island could be strong enough to penetrate the WBC to reach the coast and are suggested to contribute to the coastal Kelvin wave energy. Further north off the east coast of the Luzon Island, the eddies

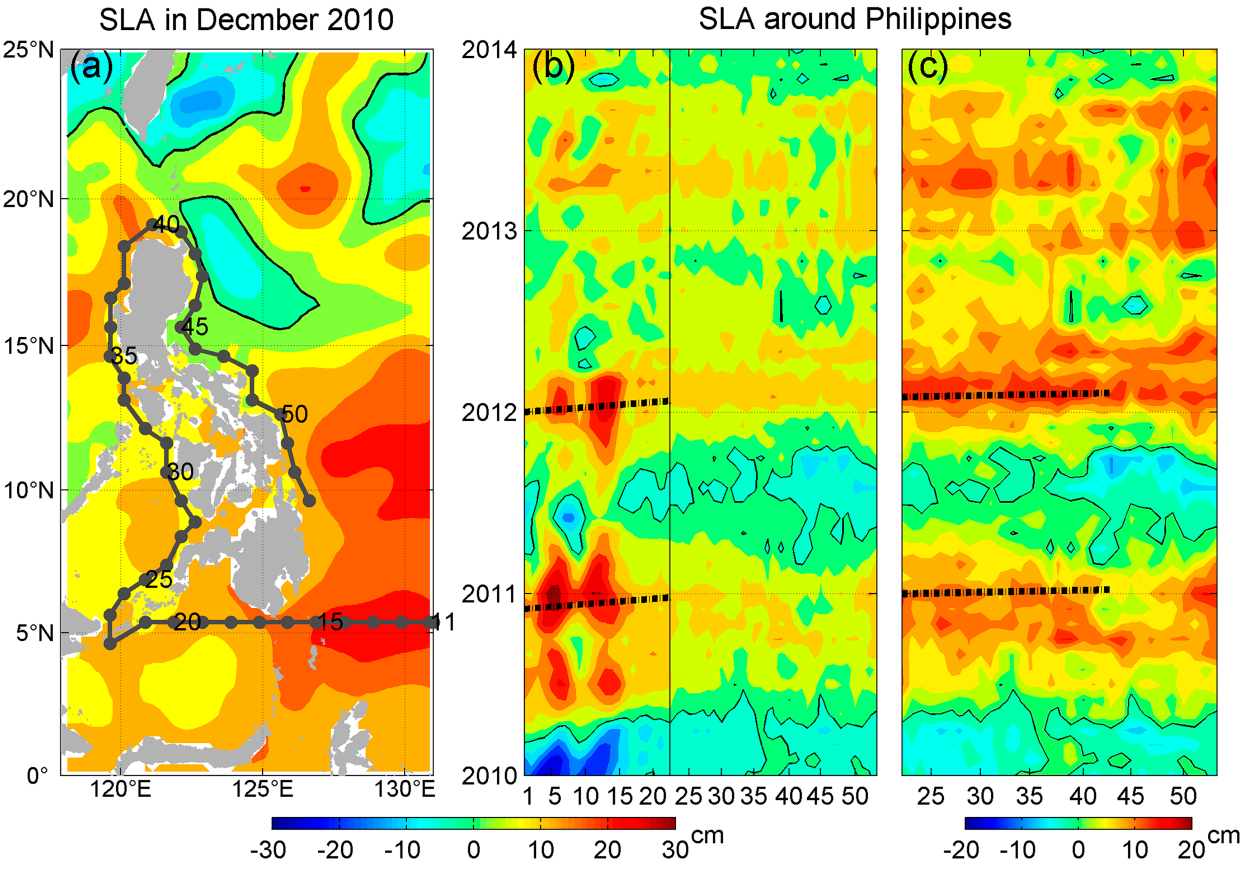

FIG. 12. (a) SLA in December 2010 and (b),(c) the Hovmöller diagram of the SLA around the Philippines. The waveguide around the Philippines is noted by a thick dotted line in (a). Stations 1–10 from 140.875° to 131.875°E with an interval of 1° along 5.375°N have been omitted. The vertical line in (b) at station 22 is the position of the Sibiu Channel. The dash lines in (b) and (c) correspond to the phase speed of the first baroclinic Rossby waves in the western tropical Pacific (~1.2 m s^{-1}) and the phase speed of the first baroclinic Kelvin waves around 8°–18°N (~3.0 m s^{-1}), respectively.

and Rossby waves are observed to be advected downstream into the Luzon Strait before reaching the boundary (Yuan et al. 2006), thus having less influence on the coastal SLA. The detailed nonlinear dynamics of the Rossby wave reflection and coastal Kelvin wave generation is beyond the scope of this study.

As gravity waves, the Kelvin waves are not easily blocked by the Kuroshio in the Luzon Strait. A theoretical coastal Kelvin wave model (Gill 1982) is employed to predict the SLA along the east coast of the Philippines from the Mindoro Strait, which provides a quantitative assessment of the Kelvin wave propagation around the archipelago. The first 10 baroclinic modes of the Kelvin waves in the model are integrated, following Hu et al. (2019), which have effectively reproduced the SLA observed by the satellite altimeter around the Philippine Archipelago (Figs. 13a,b). For example, the positive SLA during late 2010 and 2012–2013 and the negative SLA during the 2015/16 super El Niño are reproduced successfully by the Kelvin wave model. In comparison, the SLAs forced by the alongshore winds are small enough to be neglected (Fig. 13c). For instance, at the 18°N off the eastern coast of the Philippines (station 42), the standard deviation of the wind forced SLA is 0.77 cm, whereas the standard deviation induced by the Kelvin waves is 5.65 cm. Kashino et al. (2009) and Zhuang et al. (2013) have also mentioned that local wind variability in this region did not appear to contribute significantly to changes in the current system. The satellite SLA in good comparison with the simulated SLA in Fig. 13d suggests that the interannual SLAs around the Philippines are predominantly driven by the Kelvin waves north of station 50, with minor influences from local intraseasonal variations and some influences from the Rossby waves south of station 50.

The satellite- and the model-simulated SLAs show sizable differences along the east Mindanao coasts (after station 50, Fig. 13d), suggesting influences from the Rossby waves. These SLAs are part of the equatorial Rossby waves entering the Sulawesi Sea and are nearly in phase with the Kelvin waves. Only as small as ~4 cm of the Rossby wave SLAs have arrived at the coasts, which are smaller than the Kelvin wave SLA larger than 8 cm. The majority of the Rossby waves excited by the wind curl anomalies are evidently blocked by the WBCs and do not reach the coasts. The long Rossby waves do not alter the offshore pressure gradient of the boundary layer unless they are reflected into short waves. The Kelvin wave propagation

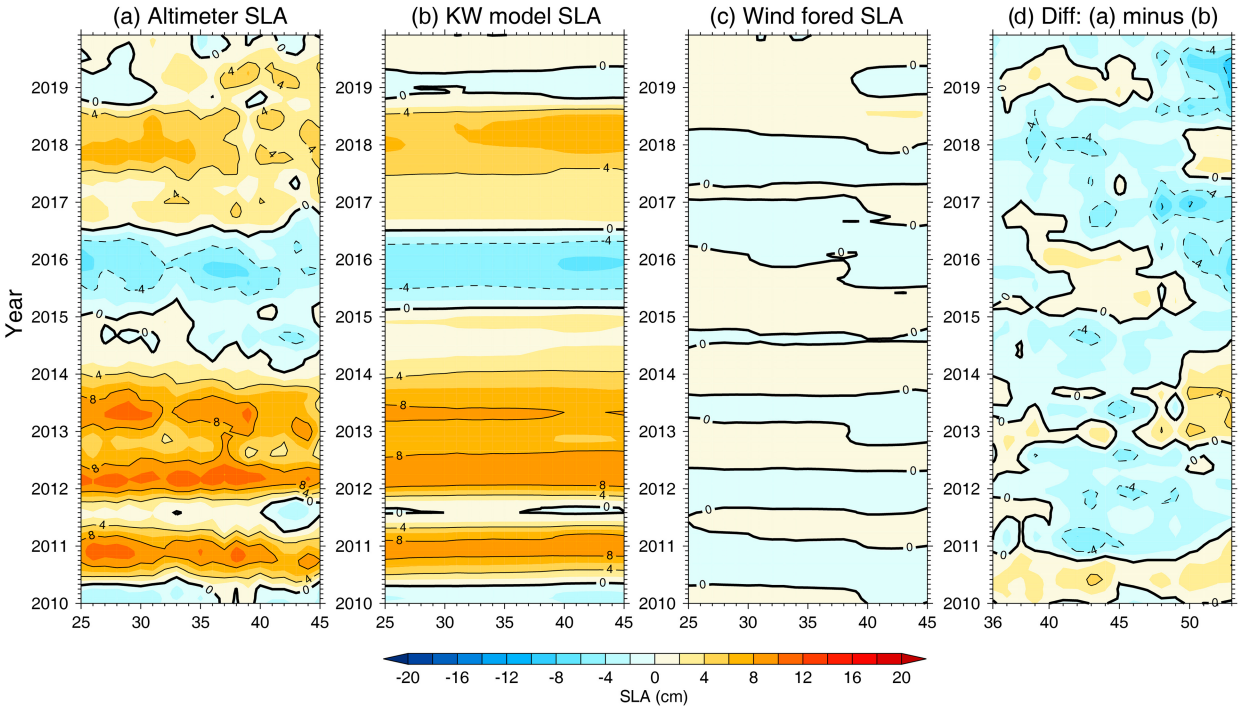

FIG. 13. Hovmöller diagram of the SLA from (a) altimeter observation, simulated by a coastally trapped (b) Kelvin wave model, and forced by the alongshore (c) wind forcing around the Philippines. (d) The difference between the satellite observed and Kelvin wave forced SLA. The diagrams have been smoothed by a 13-month Butterworth low-pass filter from the monthly data. The waveguide from stations 25 to 53 is indicated in Fig. 12a.

around the Philippine Archipelago is evidently the primary dynamics controlling the SLA at the Pacific western boundary, which would impact on the WBCs via the geostrophic balance.

The dynamics of the WBC changes are explained as the following (Fig. 14). Strong downwelling equatorial Rossby waves in the western Pacific forced by the easterly winds during the onset of the La Niña propagated westward and hit the western boundary. The sea level gradient between the equatorial western Pacific and the SCS was established, and the interactions between the MC and the Rossby waves generated nonlinear reflections of the Rossby waves with leakage into the Sulawesi Sea. The Rossby wave leakage forced Indonesian throughflow anomalies and downwelling coastal Kelvin waves to propagate clockwise around the Philippine islands. As the Kelvin waves arrived at the east Philippine coasts, the coastal sea level was elevated, generating the eastward pressure gradient and leading to southward anomalies of the WBCs via geostrophy. The situation is the opposite during El Niño events. It is worth mentioning that the energy of the Kelvin waves is likely influenced strongly by the nonlinearity of the WBC–Rossby wave interactions, as suggested by a series of theoretical and observational studies of the WBC hysteresis in the vicinity of a wide gap (Yuan et al. 2019; X. Li et al. 2021).

The dynamics provide an explanation for the disparate results in previous studies and for the distinctive variations in specific years, the results of which could form the benchmark for future analyses of the interannual variability of the Pacific low-latitude WBCs. Besides the ENSO-related SLA driving the observed WBC variability, readers are reminded of other mechanisms, such as off-equatorial eddy activity (Lien et al. 2014), local Ekman pumping (Kim et al. 2004; Ren et al. 2020), Pacific decadal oscillation phase shifts (Z. Chen et al. 2015), and interaction with the interannual SCS circulation (Liu et al. 2011; Wang et al. 2011; Wang et al. 2020), the study of which is beyond the scope of this study.

5. Conclusions

In this paper, the interannual variations of the Pacific low-latitude WBCs are investigated using hydrographic data collected during two research cruises in the winters of late 2010 and 2012, combined with satellite altimeter data, in situ mooring measurements, and numerical experiments. Observations suggest that the Kuroshio at its origin decreased significantly and the MC increased significantly during the 2010/11 La Niña peak.

The interannual WBC variations are likely generated by the propagation of coastal Kelvin waves around the Philippines during strong ENSO events, as suggested by the agreement of the Kelvin wave model simulation with the altimeter data. We suggest that, during La Niño (El Niña) events, downwelling (upwelling) Rossby waves arrive at the western equatorial Pacific to elevate (depress) the sea level in the Sulawesi Sea, which then excite downwelling (upwelling) coastal Kelvin waves to propagate into the South China Sea. These Kelvin waves propagate clockwise and raise (depress) the sea level along the east

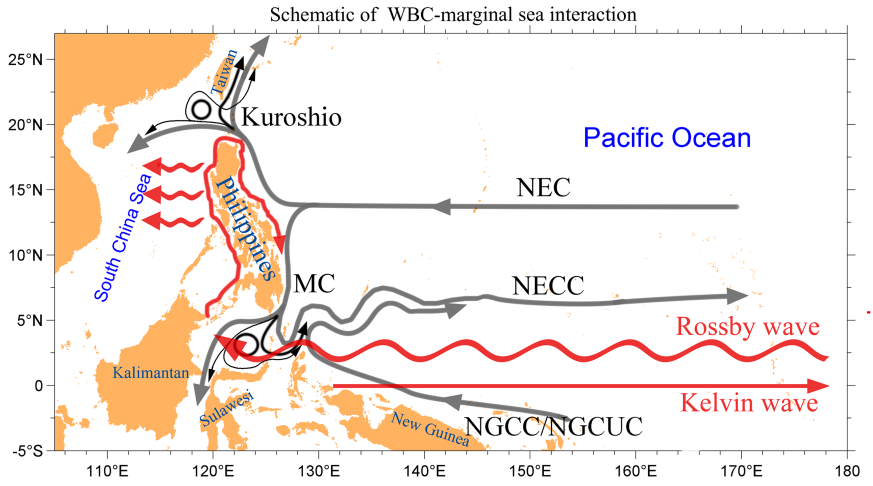

FIG. 14. Schematic of the interactions between the WBCs and the Indonesian Seas–SCS circulation. Gray arrows stand for mean circulation. Thick and thin black arrows stand for eddy shedding and penetrating states of the WBCs, respectively. Red arrows indicate wave propagation. The equatorial Rossby waves are reflected into equatorial Kelvin waves at the western boundary. Some Rossby wave energy propagates into the SCS and around the Philippines as coastal Kelvin waves while radiating Rossby waves into the northern SCS.

Philippine coasts to generate the southward (northward) anomalies of the WBCs by changing the offshore sea level gradient.

The interannual anomalies of the WBC transports are found comparable to the total geostrophic meridional transport anomalies integrated over the interior North Pacific Ocean, suggesting that the WBCs play an important role in the discharge and recharge of warm water volume of the equatorial Pacific Ocean during ENSO events.

Acknowledgments. This study was supported by the National Key Research and Development Program of China (2020YFA0608800) and the National Natural Science Foundation of China (92258301, 42106018, 91858204, and 41720104008). DY was supported by "the Taishan Scholar Program" of the Shandong Province and "the Kunpeng Outstanding Scholar Program" of the FIO/NMR of China. Affiliation 1 and affiliation 2 share the first position.

Data availability statement. The Niño-3.4 and Niño-4 index data are based on the NOAA OISST.v2 dataset, which can be downloaded from the website http://www.cpc.ncep.noaa.gov/data/indices/sstoi.indices. The ADCP data of the subsurface mooring are from the NPOCE website http://npoce.org.cn/dateAcc.aspx. The Argo profiles were from the China Argo Real-time Data Center ftp://ftp.argo.org.cn/pub/ARGO/global/. The gridded Argo data based on the Roemmich–Gilson Argo Climatology were downloaded from the website https://sio-argo.ucsd.edu/RG_Climatology.html. The absolute dynamic topography (ADT) and derived variables of the satellite product distributed by the CMEMS can be downloaded from the website https://data.marine.copernicus.eu/product/SEALEVEL_GLO_PHY_L4_MY_008_047/download?dataset=cmems_obs-sl_glo_phy-ssh_my_allsat-l4-duacs-0.25deg_P1D. Monthly wind reanalysis data provided by ERA5 ocean dataset can be downloaded from the website https://cds.climate.copernicus.eu/cdsapp#!/dataset/reanalysis-era5-single-levels-monthly-means?tab=form. The hydrographic CTD data are available on the website https://www.nsfcodc.cn/. Data and samples were collected on board R/V *Kexue-1* implementing the open research cruises NORC2010-04 (40949904) and NORC2012-09 (41149909) supported by NSFC Shiptime Sharing Project.

REFERENCES

Akima, H., 1970: A new method of interpolation and smooth curve fitting based on local procedures. *J. Assoc. Comput. Mach.*, **17**, 589–602, https://doi.org/10.1145/321607.321609.

Bretherton, C. S., M. Widmann, V. Dymnikov, J. Wallace, and I. Bladé, 1999: The effective number of spatial degrees of freedom of a time-varying field. *J. Climate*, **12**, 1990–2009, https://doi.org/10.1175/1520-0442(1999)012<1990:TENOSD>2.0.CO;2.

Chelton, D. B., R. A. deSzoeke, M. G. Schlax, K. El Naggar, and N. Siwertz, 1998: Geographical variability of the first baroclinic Rossby radius of deformation. *J. Phys. Oceanogr.*, **28**, 433–460, https://doi.org/10.1175/1520-0485(1998)028<0433:GVOTFB>2.0.CO;2.

Chen, X., B. Qiu, X. Cheng, Y. Qi, and Y. Du, 2015: Intra-seasonal variability of Pacific-origin sea level anomalies around the Philippine Archipelago. *J. Oceanogr.*, **71**, 239–249, https://doi.org/10.1007/s10872-015-0281-9.

Chen, Z., L. Wu, B. Qiu, L. Li, D. Hu, C. Liu, and X. Liang, 2015: Strengthening Kuroshio observed at its origin during November 2010 to October 2012. *J. Geophys. Res. Oceans*, **120**, 2460–2470, https://doi.org/10.1002/2014JC010590.

Chu, P. C., 1995: P-vector method for determining absolute velocity from hydrographic data. *Mar. Technol. Soc. J.*, **29**, 3–14.

Clarke, A. J., 2008: *An Introduction to the Dynamics of El Niño and the Southern Oscillation*. Academic Press, 324 pp.

Gill, A. E., 1982: *Atmosphere–Ocean Dynamics*. Academic Press, 662 pp.

Hamed, K. H., and A. Ramachandra Rao, 1998: A modified Mann-Kendall trend test for autocorrelated data. *J. Hydrol.*, **204**, 182–196, https://doi.org/10.1016/S0022-1694(97)00125-X.

Hu, D., and Coauthors, 2011: *Northwestern Pacific Ocean Circulation and Climate Experiment (NPOCE) Science/Implementation Plan*. China Ocean Press, 100 pp.

——, and Coauthors, 2013: Direct measurements of the Luzon Undercurrent. *J. Phys. Oceanogr.*, **43**, 1417–1425, https://doi.org/10.1175/JPO-D-12-0165.1.

——, and Coauthors, 2015: Pacific western boundary currents and their roles in climate. *Nature*, **522**, 299–308, https://doi.org/10.1038/nature14504.

Hu, D. X., M. C. Cui, T. D. Qu, and Y. X. Li, 1991: A subsurface northward current off Mindanao identified by dynamic calculation. *Oceanography of Asian Marginal Seas*, K. Takanao, Ed., Elsevier Oceanography Series, Vol. 54, Elsevier, 359–365, https://doi.org/10.1016/S0422-9894(08)70108-9.

Hu, S., and D. Hu, 2014: Variability of the Pacific North Equatorial Current from repeated shipboard acoustic Doppler current profiler measurements. *J. Oceanogr.*, **70**, 559–571, https://doi.org/10.1007/s10872-014-0253-5.

——, ——, C. Guan, F. Wang, L. Zhang, F. Wang, and Q. Wang, 2016: Interannual variability of the Mindanao Current/Undercurrent in direct observations and numerical simulations. *J. Phys. Oceanogr.*, **46**, 483–499, https://doi.org/10.1175/JPO-D-15-0092.1.

——, X. Lu, S. Li, F. Wang, and J. Ma, 2021: Multi-decadal trends in the tropical Pacific western boundary currents retrieved from historical hydrological observations. *Sci. China Earth Sci.*, **64**, 600–610, https://doi.org/10.1007/s11430-020-9703-4.

Hu, X., and Coauthors, 2019: Interannual variability of the Sulawesi Sea circulation forced by Indo-Pacific planetary waves. *J. Geophys. Res. Oceans*, **124**, 1616–1633, https://doi.org/10.1029/2018JC014356.

Jin, F.-F., 1997a: An equatorial ocean recharge paradigm for ENSO. Part I: Conceptual model. *J. Atmos. Sci.*, **54**, 811–829, https://doi.org/10.1175/1520-0469(1997)054<0811:AEORPF>2.0.CO;2.

——, 1997b: An equatorial ocean recharge paradigm for ENSO. Part II: A stripped-down coupled model. *J. Atmos. Sci.*, **54**, 830–827, https://doi.org/10.1175/1520-0469(1997)054<0830:AEORPF>2.0.CO;2.

Kashino, Y., A. Ishida, and Y. Kuroda, 2005: Variability of the Mindanao Current: Mooring observation results. *Geophys. Res. Lett.*, **32**, L18611, https://doi.org/10.1029/2005GL023880.

——, N. España, F. Syamsudin, K. J. Richards, T. Jensen, P. Dutrieux, and A. Ishida, 2009: Observations of the North Equatorial Current, Mindanao Current, and Kuroshio Current system during the 2006/07 El Niño and 2007/08 La Niña. *J. Oceanogr.*, **65**, 325–333, https://doi.org/10.1007/s10872-009-0030-z.

——, I. Ueki, and H. Sasaki, 2015: Ocean variability east of Mindanao: Mooring observations at 7°N, revisited. *J. Geophys. Res. Oceans*, **120**, 2540–2554, https://doi.org/10.1002/2015JC010703.

Kessler, W. S., and B. A. Taft, 1987: Dynamic heights and zonal geostrophic transports in the central tropical Pacific during 1979–84. *J. Phys. Oceanogr.*, **17**, 97–122, https://doi.org/10.1175/1520-0485(1987)017<0097:DHAZGT>2.0.CO;2.

Kim, Y. Y., T. Qu, T. Jensen, T. Miyama, H. Mitsudera, H.-W. Kang, and A. Ishida, 2004: Seasonal and interannual variations of the North Equatorial Current bifurcation in a high-resolution OGCM. *J. Geophys. Res.*, **109**, C03040, https://doi.org/10.1029/2003JC002013.

Li, B., D. Yuan, and H. Zhou, 2018: Water masses in the far western equatorial Pacific during the winters of 2010 and 2012. *J. Oceanol. Limnol.*, **36**, 1459–1474, https://doi.org/10.1007/s00343-018-6068-2.

Li, M., H. Xue, J. Wei, L. Liang, A. L. Gordon, and S. Yang, 2021: The role of the Mindoro–Sibutu Pathway on the South China Sea multilayer circulation. *J. Phys. Oceanogr.*, **51**, 2767–2782, https://doi.org/10.1175/JPO-D-20-0165.1.

Li, X., and Coauthors, 2021: Moored observations of currents and water mass properties between Talaud and Halmahera Islands at the entrance of the Indonesian seas. *J. Phys. Oceanogr.*, **51**, 3557–3572, https://doi.org/10.1175/JPO-D-21-0048.1.

Lien, R.-C., B. Ma, Y.-H. Cheng, C.-R. Ho, B. Qiu, C. M. Lee, and M.-H. Chang, 2014: Modulation of Kuroshio transport by mesoscale eddies at the Luzon Strait entrance. *J. Geophys. Res. Oceans*, **119**, 2129–2142, https://doi.org/10.1002/2013JC009548.

Lindstrom, E., R. Lukas, R. Fine, E. Firing, S. Godfrey, G. Meyers, and M. Tsuchiya, 1987: The western equatorial Pacific Ocean circulation study. *Nature*, **330**, 533–537, https://doi.org/10.1038/330533a0.

Liu, Q., M. Feng, and D. Wang, 2011: ENSO-induced interannual variability in the southeastern South China Sea. *J. Oceanogr.*, **67**, 127–133, https://doi.org/10.1007/s10872-011-0002-y.

Liu, Y., Q. Ren, F. Yu, C. Wei, X. Diao, and F. Nan, 2023: The vertical structure and variability of currents east of Philippines from mooring measurements during the 2015/2016 El Niño. *Front. Mar. Sci.*, **10**, 1113525, https://doi.org/10.3389/fmars.2023.1113525.

Lukas, R., 1988: Interannual fluctuations of the Mindanao Current inferred from sea level. *J. Geophys. Res.*, **93**, 6744–6748, https://doi.org/10.1029/JC093iC06p06744.

——, E. Firing, P. Hacker, P. L. Richardson, C. A. Collins, R. Fine, and R. Gammon, 1991: Observations of the Mindanao Current during the western equatorial Pacific Ocean circulation study. *J. Geophys. Res.*, **96**, 7089–7104, https://doi.org/10.1029/91JC00062.

Ma, J., S. Hu, D. Hu, C. Villanoy, Q. Wang, X. Lu, and X. Yuan, 2022: Structure and variability of the Kuroshio and Luzon Undercurrent observed by a mooring array. *J. Geophys. Res. Oceans*, **127**, e2021JC017754, https://doi.org/10.1029/2021JC017754.

Metzger, E. J., and H. E. Hurlburt, 1996: Coupled dynamics of the South China Sea, the Sulu Sea, and the Pacific Ocean. *J. Geophys. Res.*, **101**, 12 331–12 352, https://doi.org/10.1029/95JC03861.

Meyers, G., 1979: Annual variation in the slope of the 14°C isotherm along the equator in the Pacific Ocean. *J. Phys. Oceanogr.*, **9**, 885–891, https://doi.org/10.1175/1520-0485(1979)009<0885:AVITSO>2.0.CO;2.

Munk, W. H., 1950: On the wind-driven ocean circulation. *J. Meteor.*, **7**, 80–93, https://doi.org/10.1175/1520-0469(1950)007<0080:OTWDOC>2.0.CO;2.

Nitani, H., 1972: Beginning of the Kuroshio. *Kuroshio: Physical Aspects of the Japan Current*, University of Tokyo Press, 129–163.

Qiu, B., and R. Lukas, 1996: Seasonal and interannual variability of the North Equatorial Current, the Mindanao Current, and the Kuroshio along the Pacific western boundary. *J. Geophys. Res.*, **101**, 12 315–12 330, https://doi.org/10.1029/95JC03204.

——, and S. Chen, 2010: Interannual-to-decadal variability in the bifurcation of the North Equatorial Current off the Philippines. *J. Phys. Oceanogr.*, **40**, 2525–2538, https://doi.org/10.1175/2010JPO4462.1.

Qu, T., and R. Lukas, 2003: The Bifurcation of the North Equatorial Current in the Pacific. *J. Phys. Oceanogr.*, **33**, 5–18, https://doi.org/10.1175/1520-0485(2003)033<0005:TBOTNE>2.0.CO;2.

——, H. Mitsudera, and T. Yamagata, 1998: On the western boundary currents in the Philippine Sea. *J. Geophys. Res.*, **103**, 7537–7548, https://doi.org/10.1029/98JC00263.

——, ——, and ——, 1999: A climatology of the circulation and water mass distribution near the Philippine Coast. *J. Phys. Oceanogr.*, **29**, 1488–1505, https://doi.org/10.1175/1520-0485(1999)029<1488:ACOTCA>2.0.CO;2.

Ren, Q., Y. Li, F. Wang, J. Duan, S. Hu, and F. Wang, 2020: Variability of the Mindanao Current induced by El Niño events. *J. Phys. Oceanogr.*, **50**, 1753–1772, https://doi.org/10.1175/JPO-D-19-0150.1.

Roemmich, D., and J. Gilson, 2009: The 2004–2008 mean and annual cycle of temperature, salinity, and steric height in the global ocean from the Argo Program. *Prog. Oceanogr.*, **82**, 81–100, https://doi.org/10.1016/j.pocean.2009.03.004.

Sarachik, E. S., and M. A. Cane, 2010: *The El Niño-Southern Oscillation Phenomenon*. Cambridge University Press, 384 pp.

Sprintall, J., A. L. Gordon, R. Murtugudde, and R. D. Susanto, 2000: A semiannual Indian Ocean forced Kelvin wave observed in the Indonesian seas in May 1997. *J. Geophys. Res.*, **105**, 17 217–17 230, https://doi.org/10.1029/2000JC900065.

Stommel, H., 1948: The westward intensification of wind-driven ocean currents. *Eos, Trans. Amer. Geophys. Union*, **29**, 202–206, https://doi.org/10.1029/TR029i002p00202.

Sverdrup, H. U., 1947: Wind-driven currents in a baroclinic ocean; with application to the equatorial currents of the eastern Pacific. *Proc. Natl. Acad. Sci. USA*, **33**, 318–326, https://doi.org/10.1073/pnas.33.11.318.

Toole, J. M., R. C. Millard, Z. Wang, and S. Pu, 1990: Observations of the Pacific North Equatorial Current bifurcation at the Philippine Coast. *J. Phys. Oceanogr.*, **20**, 307–318, https://doi.org/10.1175/1520-0485(1990)020<0307:OOTPNE>2.0.CO;2.

Wang, Q., and Coauthors, 2020: Interannual variability of South China Sea winter circulation: Response to Luzon Strait transport and El Niño wind. *Climate Dyn.*, **54**, 1145–1159, https://doi.org/10.1007/s00382-019-05050-2.

Wang, Q.-y., and D.-x. Hu, 2006: Bifurcation of the North Equatorial Current derived from altimetry in the Pacific Ocean. *J. Hydrodyn.*, **18**, 620–626, https://doi.org/10.1016/S1001-6058(06)60144-3.

Wang, W., D. Wang, W. Zhou, Q. Liu, Y. Yu, and C. Li, 2011: Impact of the South China Sea throughflow on the Pacific low-latitude western boundary current: A numerical study for seasonal and interannual time scales. *Adv. Atmos. Sci.*, **28**, 1367–1376, https://doi.org/10.1007/s00376-011-0142-4.

Wijffels, S., E. Firing, and J. Toole, 1995: The mean structure and variability of the Mindanao Current at 8°N. *J. Geophys. Res.*, **100**, 18 421–18 435, https://doi.org/10.1029/95JC01347.

Wyrtki, K., 1961: Physical oceanography of the Southeast Asian waters. Vol. 2, University of California, San Diego NAGA Rep., 195 pp.

Yuan, D., and Z. Wang, 2011: Hysteresis and dynamics of a western boundary current flowing by a gap forced by impingement of mesoscale eddies. *J. Phys. Oceanogr.*, **41**, 878–888, https://doi.org/10.1175/2010JPO4489.1.

——, W. Han, and D. Hu, 2006: Surface Kuroshio path in the Luzon Strait area derived from satellite remote sensing data. *J. Geophys. Res.*, **111**, C11007, https://doi.org/10.1029/2005JC003412.

——, Z. Zhang, P. C. Chu, and W. K. Dewar, 2014: Geostrophic circulation in the tropical North Pacific Ocean based on Argo profiles. *J. Phys. Oceanogr.*, **44**, 558–575, https://doi.org/10.1175/JPO-D-12-0230.1.

——, X. Song, Y. Yang, and W. K. Dewar, 2019: Dynamics of mesoscale eddies interacting with a western boundary current flowing by a gap. *J. Geophys. Res. Oceans*, **124**, 4117–4132, https://doi.org/10.1029/2019JC014949.

Zhai, F., and D. Hu, 2013: Revisit the interannual variability of the North Equatorial Current transport with ECMWF ORA-S3. *J. Geophys. Res. Oceans*, **118**, 1349–1366, https://doi.org/10.1002/jgrc.20093.

Zhang, L., D. Hu, S. Hu, F. Wang, F. Wang, and D. Yuan, 2014: Mindanao Current/Undercurrent measured by a subsurface mooring. *J. Geophys. Res. Oceans*, **119**, 3617–3628, https://doi.org/10.1002/2013JC009693.

Zhuang, W., B. Qiu, and Y. Du, 2013: Low-frequency western Pacific Ocean sea level and circulation changes due to the connectivity of the Philippine Archipelago. *J. Geophys. Res. Oceans*, **118**, 6759–6773, https://doi.org/10.1002/2013JC009376.